Hindawi
Journal of Nanomaterials
Volume 2021, Article ID 5582737, 7 pages
https://doi.org/10.1155/2021/5582737

Research Article

Synthesis of Hybrid Lead Iodide Perovskite Thin Film by Two-Step Method Modified with a Double Dipping Circle to Control Its Crystallization and Morphology to Improve Solar Cells' Performance

Huy Anh Dinh,[1,2] Thuy Thanh Thi Nguyen,[1,2] Le Thi Nguyen,[1,2] Hai Tri Nguyen,[1,2] Dien Minh Trinh,[1,2] Vy Anh Tran,[1,2] and Phuong Tuyet Nguyen [1,2]

[1]*Faculty of Chemistry, University of Science, Ho Chi Minh City, Vietnam*
[2]*Vietnam National University Ho Chi Minh City, Vietnam*

Correspondence should be addressed to Phuong Tuyet Nguyen; ntphuong@hcmus.edu.vn

Received 6 January 2021; Revised 29 January 2021; Accepted 2 February 2021; Published 16 February 2021

Academic Editor: Mai Duy Hien

Crystallization and morphology of perovskite film played an important role to obtain efficient performance of perovskite solar cells. This study is aimed at optimizing the fabrication of hybrid organic–inorganic lead iodide perovskite layer by a two-step method modified by a double dip coating process which enables to control the perovskite crystallization and morphology. The duration time of each circle for the step of dipping PbI_2 film to methylammonium iodide solution was varied from 90 to 240 second. The obtained perovskite films were characterized by X-ray diffraction to evaluate the transformation of PbI_2 reactant to the perovskite product and its crystallization, by scanning electron microscopy to observe its morphology. Then, the perovskite films were implemented in functional perovskite solar cell devices followed by current–voltage characterization. Results showed that the perovskite was formed via an equilibrium process which reached an optimum transformation of PbI_2 to the product after 2×150 second circle dip coating, and its morphology was smooth with the least voids. The solar cell devices fabricated at the optimum conditions achieved a comparable performance of about 14%.

1. Introduction

Organic–inorganic hybrid materials adopting perovskite structure have attracted considerable attention because of their superior properties and excellent power conversion efficiencies (PCE). The first hybrid perovskite based on $CH_3NH_3PbBr_3$ was reported by Kojima et al. with PCE value of 2.2% [1, 2]. In 2009, they obtained a PCE of 3.8% by using iodine (I) instead of bromine (Br) [2]. Later, there have been tremendous efforts to enhance the efficiency in the hybrid lead halide perovskite $CH_3NH_3PbX_3$ (X : halogen) [3–8]. Among them, Gratzel et al. reported a remarkable record on the solid-state heterojunction DSCs employing $CH_3NH_3PbI_3$ with 9.7% of PCE [4]. Recently, the PCEs of PSCs have soared to 25.2% in 2019, the highest reported to date [9]. As demonstrated in these studies, controlling the morphology of perovskite films is essential for improving the performance of PSCs. In this regard, deposition process plays an important role in the growth of perovskite crystal. In terms of fabrication processes, the solution deposition of perovskite films has been conducted through one-step and two-step approaches. One-step coating uses a solution comprising of CH_3NH_3I and PbI_2 sources, which is dissolved into a single solution, and then, it was coated on the substrate via spin-coating [4, 10, 11]. Even though the one-step deposition is simple, the challenge of obtaining the high photovoltaic performance still remains. This obstacle is largely due to the low reaction conversion, low crystallization, high pinhole density, and high series resistance [12–14].

By contrast, the two-step sequential dipping deposition pathway in fabricating the perovskite layer involves a spin-coating process to deposit lead iodide (PbI_2) onto the

substrate; then, PbI_2 film is converted into methylammonium lead iodide ($MAPbI_3$) perovskite film by dipping it in methylammonium iodide (MAI) solution followed by a heat treatment step. In 2015, Fu et al. proposed about the dissolution-recrystallization mechanism in perovskite film [15], suggesting that the reaction between PbI_2 and $MAPbI_3$ was reversible as well as the photovoltaic performance of the device was affected by this process. Later, Lou et al. [16] precisely demonstrated influence of the perovskite morphology on the device's performance through current–voltage ($J - V$) characterization. Moreover, Hsieh et al. [17] explained their experimental phenomenon based on the aforementioned mechanism and provided more evidences about the correlation of morphology evolution and crystal growth followed the dipping time, as well as their effect on the photovoltaic performance. Therefore, it is crucial to control the morphology and the transformation yield by optimizing the dipping time in order to obtain an efficient perovskite thin film for solar cell application. Recently, Gao et al. [18] reconfirmed that the soaking time is the strong factor in controlling the crystallization of $MAPbI_3$ crystal and optical properties through the UV-Vis absorbance spectra and the XRD diffraction patterns. It has been noticed that the duration of dipping time was mostly reported as total time for a whole process in literatures, and the transformation process from PbI_2 to $MAPbI_3$ perovskite occurred obviously fast [15–18]. Wei et al. demonstrated that dipping the PbI_2 film in MAI solution in a short time (less than 1 min) could form the perovskite product but just as a skin on PbI_2, but doing the same procedure in a longer time (several min) caused a fact of recrystallization of the perovskite [17]. Both situations led to low energy conversion efficiency in the solar cells. Based on all the aforementioned work, we proposed that the formation of the perovskite film should be divided into two steps including crystal nucleation and preferable oriented crystal growth. The first circle in the dipping step is aimed at creating the perovskite skin on the PbI_2 and the second circle forced to a complete transformation of the inner reactant to the product.

Herein, we report a two-step deposition method modified by a double dip coating process in perovskite film fabrication which enabled to improve the perovskite films with high crystallinity and smooth morphology. In order to evaluate the effect of dip coating treatment, we conducted experiments with different duration times of each circle (90 s, 120 s, 150 s, 180 s, and 240 s). The perovskite film was fabricated via the new modified double cycle process and characterized using various structural and electrical characterization methods. The films were then implemented in the solar cell devices which were characterized by current–voltage ($J - V$) curve measurement to evaluate their photovoltaic performance.

2. Experimental Section

2.1. Synthesis of CH_3NH_3I (MAI). MAI was prepared by following the procedure reported in literature [17]. Hydroiodic acid (57 wt. % in water, Sigma–Aldrich) was added dropwise to methylamine solution (33 wt. % in absolute ethanol, Sigma–Aldrich), and the mixture was stirred under a nitrogen flow for two hours to obtain white precipitate of MAI. The product was finally collected and dried at 45°C in a vacuum oven overnight after recrystallization in ethanol and diethyl ether at -7°C for ten hours.

2.2. Solar Cell Fabrication. Fluorine-doped tin oxide (FTO) glass (2.2 mm; 8Ω/sq; Pilkington, USA) was cleaned step by step in a detergent solution, deionized water (DI) and ethanol and acetone, rand dried by an air blower. After that, the TiO_2 compact layer (c-TiO_2) was spin-coated onto the FTO substrate with a solution of 0.15 M titanium diisopropoxide bis(acetylacetonate) (75 wt% in isopropanol) (Sigma-Aldrich, Germany) and annealed at 500°C for 30 min. The c-TiO_2 | FTO film was pretreated in a 40 mM $TiCl_4$ (≥98%, Fluka, Japan) solution at 70°C in an oven for 30 min and annealed at 500°C in 30 min. Next, a 200 nm thick mesoporous TiO_2 layer (m-TiO_2) was deposited on top of the c-TiO_2 layer by spin-coating with an ethanol-diluted commercial TiO_2 paste 30 NR (Dyesol, Australia), then calcinated from 325°C to 500°C for 2 h. The m-TiO_2 | c-TiO_2 | FTO substrate was treated again with $TiCl_4$ solution as aforementioned.

The perovskite film was then fabricated on the top of m-TiO_2 layer with the first step of loading the 1.5 M PbI_2 (Sigma–Aldrich, Germany) solution dissolved in a mixture solvent of DMF : DMSO (9 : 1) by spin-coating. Following the conventional two-step procedure, the wet PbI_2 layer was heated at 70°C for 10 min before dipping the whole substrate into the MAI solution in *iso*-propanol (9.5 mg/mL) to form the perovskite $MAPbI_3$ films, followed by a spin-coating to dry out the solvent on the surface. The dipping step was repeated two times until the perovskite film changed to dark brown; after that, it was heated on the hot plate at 120°C for 20 min. The dipping duration time for each circle was varied between 90, 120, 150, 180, and 240 seconds. It should be noted that the fabrication of PbI_2 and perovskite film was performed in ambient conditions with humidity controlled at around 30–40%.

The hole transport material (HTM) solution was prepared by dissolving 75 mM spiro-OMeTAD, 25 mM Li-TFSI, and 120 mM 4-*tert*-butylpyridine in chlorobenzene. All of these chemicals and the above solvents were purchased from Sigma–Aldrich, Germany, and used as received. Then, the HTM solution was spin-coated onto the hybrid perovskite film, and finally, a 80–100 nm gold layer was thermally evaporated on the spiro-OmeTAD-coated film to form the back contact layer. The size of one device was 1.5 × 8.7 mm. The perovskite device fabrication process was summarized in Scheme 1 with a photo of the final real device.

2.3. Material and Device Characterization. Morphology of perovskite films were obtained by field emission scanning electron microscopes (FE-SEM), operated at an accelerating voltage of 5 kV (SU-8010, Hitachi Japan). The powder X-ray diffraction (XRD) patterns of the samples were acquired using a D2 Bruker diffractometer operating at 40 kV and 150 mA, equipped with Cu $K_{\alpha 1}$ radiation source ($\lambda = 1.5406$ nm Å). The 2θ angular domain varied between 10° and 45°,

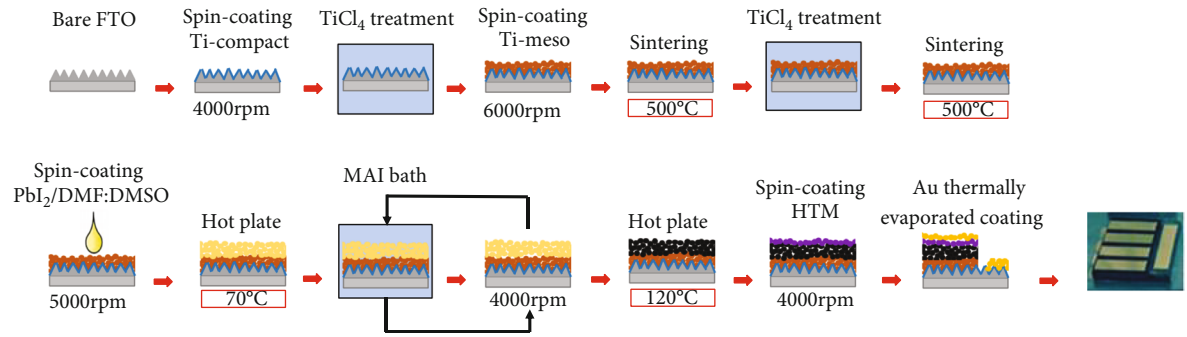

Scheme 1: The process of perovskite solar cell fabrication by two-step procedure modified double dip coating step (rpm: round per minute) with the final real device.

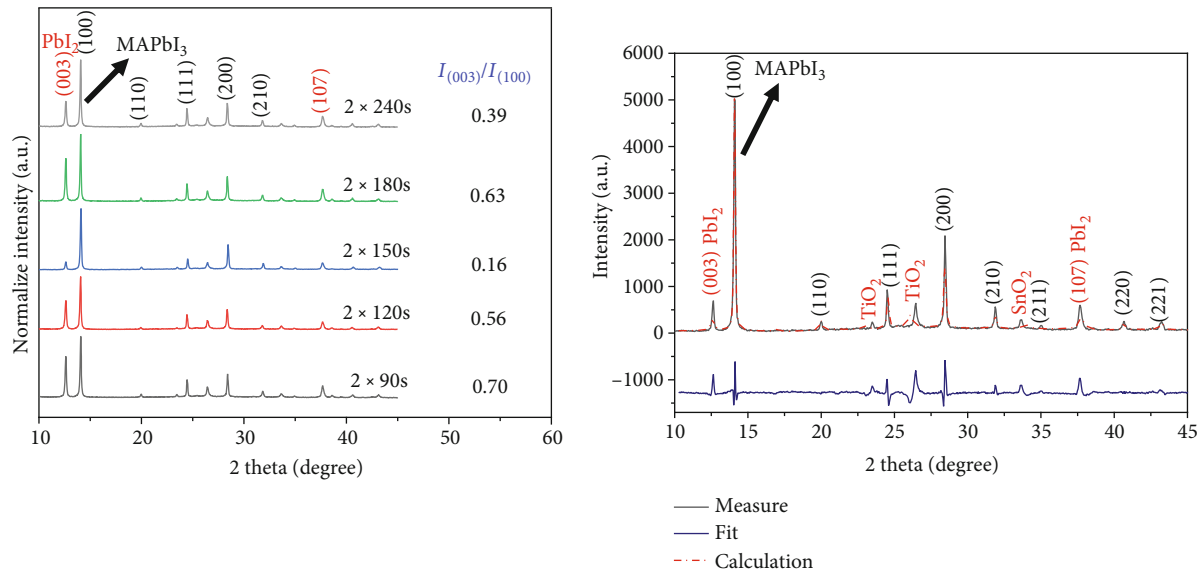

(a) (b)

Figure 1: (a) XRD patterns of $MAPbI_3$ films obtained at different conditions of dipping time $n_{dipping}$ × dipping time $t_{dipping}$. The right column gives the intensity ratios between PbI_2 (003) and $MAPbI_3$ (100). (b) Profile matching of the XRD pattern recorded on 2 × 150 s dipping condition. The structure of $MAPbI_3$ is indexed in the space group Pm-3 m, $a = b = c = 6.2673$ Å.

with a step of 0.02° and acquisition time of 0.25 s/step, and the profile matching were performed on the recorded XRD patterns, using FullProf Suite (Cu_α K-alpha1 radiation ($\lambda = 1.5406$ nm Å). Furthermore, the crystallite sizes were calculated by applying Debye-Scherrer's equation: $D_p = K\lambda/(B\ \cos\theta)$ from the XRD pattern, and the FWHM was calculated by OriginPro software.

The current–voltage (J – V) curve were measured by a Keithley 2400 digital source meter under AM 1.5G illumination and at an intensity of 100 mW cm^{-2} (Peccel Technologies, PEC-L15), while the step scan was controlled at 10 mV and the delay time was 50 ms.

Table 1: The ratio between integrated peak PbI_2 (003) and $MAPbI_3$ (100) and the calculated crystallite sizes of $MAPbI_3$ fabricated at various dipping times.

	2 × 90 s	2 × 120 s	2 × 150 s	2 × 180 s	2 × 240 s
I_{PbI_2}/I_{MAPbI_3} (*)	0.70	0.56	0.16	0.63	0.39
Crystallite size (nm)	58.90	57.06	58.08	61.05	60.71

(*) $I_{PbI_2(003)}/I_{MAPbI_3(100)}$ was calculated based on the integrated peak of PbI_2 (003) and the integrated peak of $MAPbI_3$ (100).

3. Results and Discussion

Figure 1 shows the XRD diagram of the perovskite films fabricated at different dipping times and the fitted XRD pattern of the 2 × 150 s sample which reached to the highest transformation of PbI_2 to the perovskite product. From the XRD patterns, the crystallite size of the perovskite, calculated by Debye–Scherrer's equation, and the conversion of PbI_2 layer to $MAPbI_3$ by dipping the PbI_2 film into MAI solution was shown in Table 1.

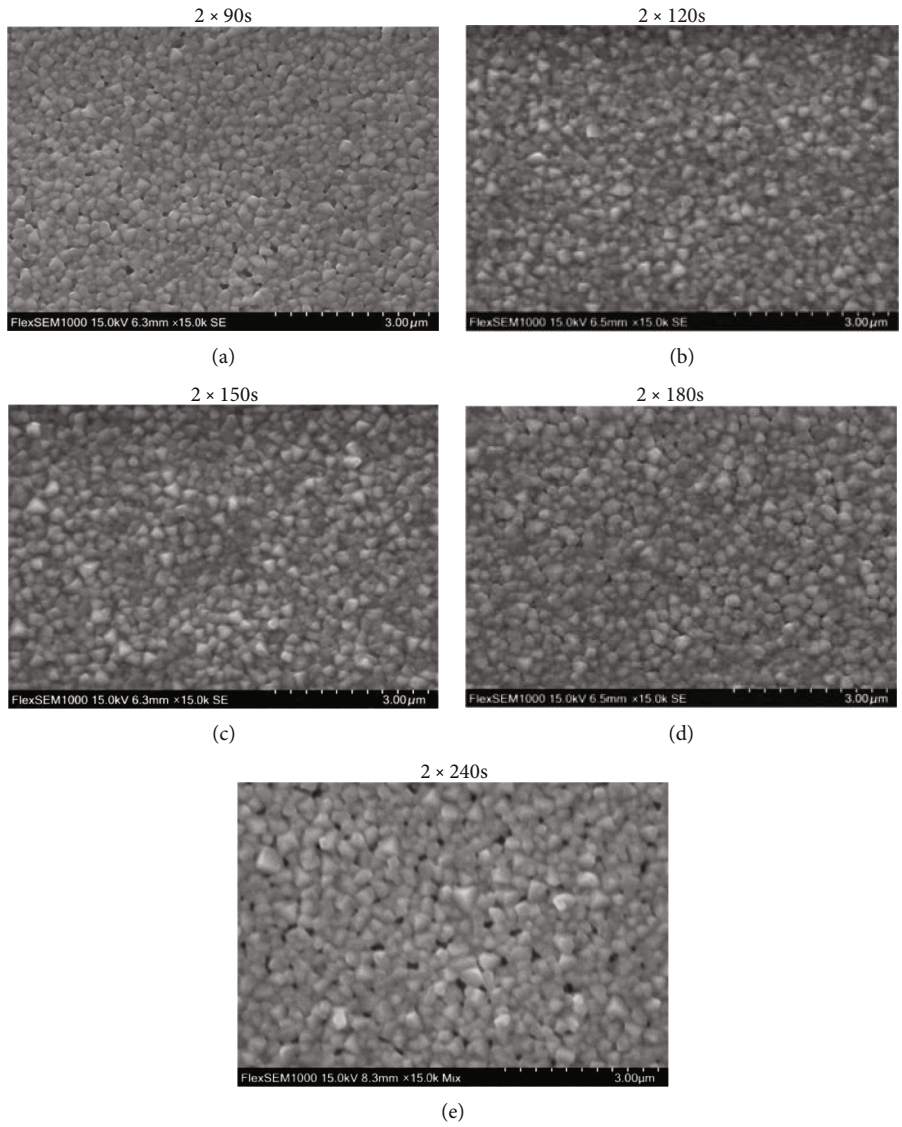

Figure 2: Scanning electron microscopy (SEM) images of the $MAPbI_3$ film fabricated at different preparation conditions: (a) 2×90 s, (b) 2×120 s, (c) 2×150 s, (d) 2×180 s, and (e) 2×240 s.

The formation of perovskite layer during the dipping process could be realized by the color changing of PbI_2 film from yellow to brown, then dark brown. We have noticed that during the single-dipping process of PbI_2 thin film to MAI solution, the color of PbI_2 film was changed slightly from yellow to a mixture of orange and brown. However, the color of the samples conducted under double dipping condition changed into brown, indicating the improvement of $MAPbI_3$ formation yield. As shown in the XRD pattern in Figure 1(a), five preferable peaks located at 14.11°, 20.02°, 24.58°, 28.46°, and 31.9° are indexed as the $MAPbI_3$ cubic phase of (100), (110), (111), (200), and (210) lattice planes, respectively [19]. However, the residual PbI_2 are observed in the XRD diffraction pattern of all samples, due to the presence of mainly (003) lattice planes at 12.7°. Moreover, as shown in Figure 1(b), some small diffraction peaks are observed at 23.48°, 26.45°, and 33.68°, which attributed to the presence of TiO_2 and SnO_2 in the sample during the synthesis approach on FTO | TiO_2 substrate [20].

Dissolution:

$$CH_3NH_3PbI_3(s) + I^- \rightarrow CH_3NH_3+ + PbI_4^{2-}$$

$$PbI_2 + 2I^- \rightarrow PbI_4^{2-}$$

Recrystallization:

$$PbI_4^- + CH_3NH_3^+ \rightarrow CH_3NH_3PbI_3 + I^-$$

Scheme 2: The proposed mechanism of dissolution–recrystallization process of perovskite film fabricated by a two-step dipping process explains the formation of voids and defects on the perosvkite film and the large grain size of perovskite crystals [17].

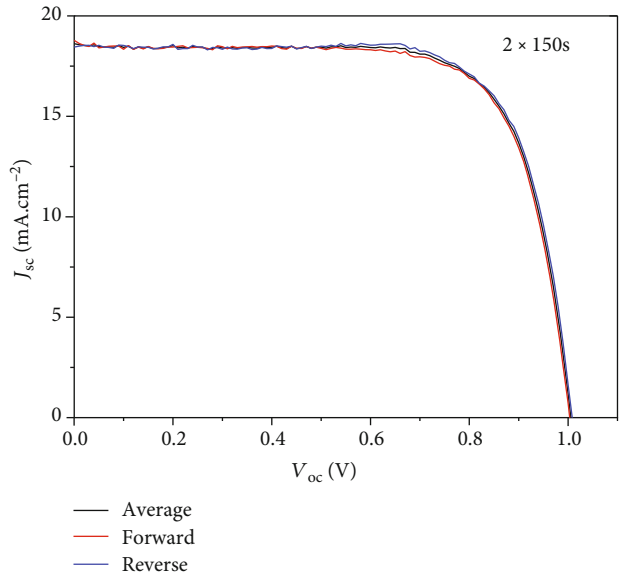

	J_{sc} (mA.cm^{-2})	V_{oc}(V)	FF	PCE (%)
Forward	19.39	1.00	0.73	14.06
Reverse	18.89	1.00	0.75	14.18
Average	19.14	1.00	0.74	14.11

(a)

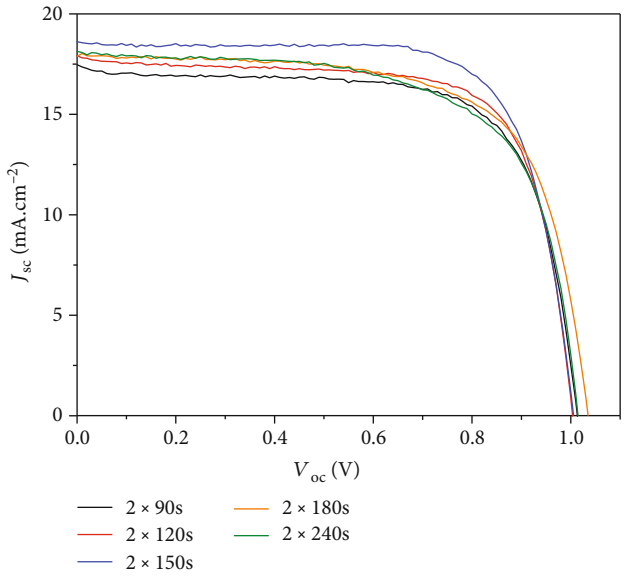

(b)

FIGURE 3: (a) $J - V$ curve of the best performance cell at 2×150 s condition measured under AM 1.5G illumination at 100 mW cm^{-2} with forward and reverse scanning. (b) $J - V$ curves of the best devices fabricated at various dipping times.

The ratio of PbI_2/$MAPbI_3$ is found to decrease significantly from 0.7 to 0.16 when the dipping time per circle was varied from 90 s to 150 s, but then increases to 0.63 when the dipping time was prolonged to 180 s. It indicates that the reaction between PbI_2 and MAI is a reversible process, and the highest conversion of PbI_2 is obtained at 2×150 s dipping time. The results in Table 1 also clearly show that the average crystal size (D) increases when varying the reaction time from 90 s to 240 s.

In order to study the influence of the dipping time on the growth of the $MAPbI_3$ grain size as well as the dissolution-recrystallization process on the $MAPbI_3$ surface, the SEM analysis of fabricated perovskite film was examined at different conditions. After reaction at 2×90 s, the surface morphology of crystallites $MAPbI_3$ are covered in regularly shaped grains ~100 nm in diameter (Figure 2(a)), and the holes are observed on the perovskite film. After 2×120 s and 2×150 s dipping in MAI solution, the perovskite films are composed of regularly grains with size of 150–300 nm which can cover all holes and defects on the perovskite surface (Figures 2(b) and 2(c)). However, the SEM image of the samples obtained at 2×180 s and 2×240 s provides average grain sizes of 150–300 nm and 150–400 nm, respectively (Figures 2(d) and 2(e)) as well as the presence of holes on the surface even though the duration time was prolonged. This observation might be explained by the dissolution–recrystallization process of $MAPbI_3$, which was reported to occur not only on the layer of perovskite film but also inside of the perovskite grains, due to the oversaturation of I^- ion [15, 17]. Hence, the formed $MAPbI_3$ will react with an excess amount of I^- ion in $MAPbI_3$ solution and generated to lead polyiodide complex (PbI_4^{2-}) as well as the unconverted PbI_2. Accordingly, PbI_4^{2-} will react with $CH_3NH_3^+$ ion and recrystallize to grow the perovskite grain, as shown in Scheme 2.

The impact of the double dipping process on the photovoltaic performance of the PSCs is shown in Figure 3 and Table 2. The $J - V$ curves under forward and reverse scanning (Figure 3(a)) are reproducible indicating that the device works reasonably well under the measurement conditions, and it performs stable photovoltaic properties. The same observation was obtained for all the devices fabricated at various conditions. When the dipping time is increased from 2×90 to 2×240 s, the short-circuit density (J_{sc}) increases gradually and then decreases, reaching a highest value (19.01 mA.cm^{-2}) at 2×150 s, which exhibits the balance between the conversion of PbI_2 to $MAPbI_3$ and dissolution process (Table 2). The fill factor of these solar cells keeps almost constant from 0.73 at 2×90 s to 0.71 at 2×150 s and then decreased significantly to 0.66 at 2×180 s and 0.68 at 2×240 s. Besides, the results show that the overall conversion efficiency increases dramatically from 12.8% at 2×90 s to 13.4% at 2×150 s, then reduces to 11.8% at 2×180 s. These results imply that the double dipping process enhances the conversion of PbI_2 to $MAPbI_3$ and its morphology, which are important factors to improve the electrical optical properties of the perovskite. The solar cell devices prepared at 2×150 s double dip coating process, which is

Table 2: Photovoltaic performance parameters of the solar cell devices assembled at different dipping times.

Dipping time	J_{sc} (mA.Cm^{-2})	V_{oc} (V)	FF	η (%)
2 × 90 s	17.23 ± 0.64	1.03 ± 0.02	0.73 ± 0.03	12.86 ± 0.62
2 × 120 s	17.55 ± 0.60	1.00 ± 0.01	0.71 ± 0.03	12.37 ± 0.64
2 × 150 s	19.01 ± 0.65	1.00 ± 0.01	0.71 ± 0.04	13.43 ± 0.86
2 × 180 s	17.90 ± 0.19	1.01 ± 0.01	0.66 ± 0.01	11.81 ± 0.39
2 × 240 s	17.6 ± 0.51	1.01 ± 0.02	0.68 ± 0.01	12.30 ± 0.33

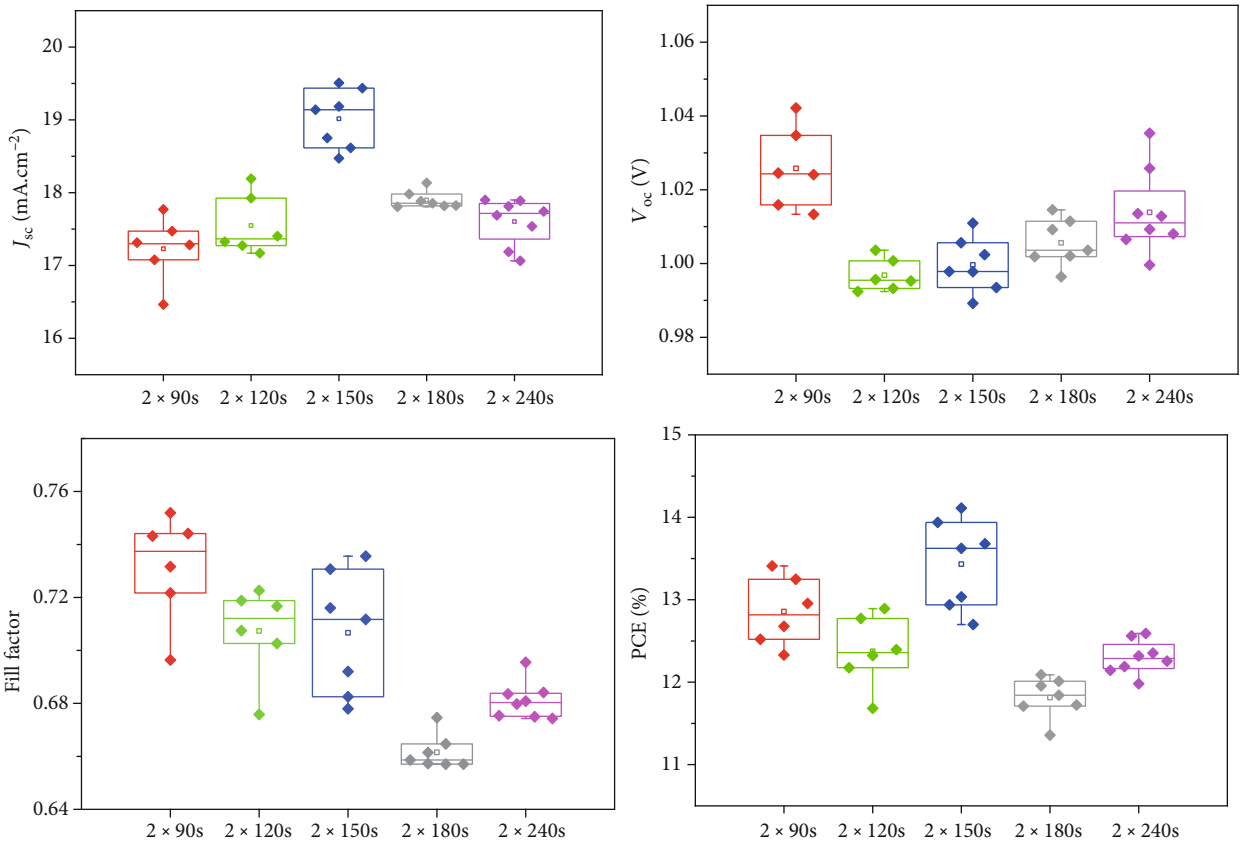

Figure 4: The statistical analysis of current density (J_{sc}), open circuit voltage (V_{oc}), fill factor, and power conversion efficiency (PCE) of all the solar cell devices fabricated at different double dipping conditions.

optimized conditions, show impressive photovoltaic performance of 14%. The results are comparable among reported ones focused on the perovskite material of $MAPbI_3$ in literature [15–20].

It can be clearly seen in Figure 4 that the 2 × 150 s solar cells could reach the optimum efficiency mostly due to the record of J_{sc} values which is mainly affected by the formation of the perovskite film. The high quality of the perovskite layer determined by the high transformation yield of the reactant PbI_2 to $MAPbI_3$ and smooth morphology of the perovskite film with no defects and high crystallinity is the key factor to optimize the performance of the solar cells. The double dipping process shows to be a suitable method to control the formation of the $MAPbI_3$ perovskite. The first circle helped to create perovskite on the surface and the nucleus crystal inside. The second circle improved the crystallization of the product deep inside the film. With the optimum duration time for each circle at 150 s, the perovskite could form at the maximum yield, and the dissolution as well as the recrystallization on the surface did not have adequate time to occur, leading to a smooth morphology with no voids and no defects.

4. Conclusion

The present work focused on the optimization of the two-step process modified by double dipping circle to produce

high superior hybrid lead iodide perovskite solar cells. The $MAPbI_3$ surface layer with high crystallinity and fewer defects was successfully prepared via an equilibrium transformation of PbI_2 at optimized dipping time. XRD analysis revealed the impact of the dipping time onto the conversion of PbI_2 to $MAPbI_3$, which is an important factor to achieve a reasonable device performance. SEM images exhibited the different morphology features of the $MAPbI_3$ layer prepared from different dipping times. SEM results implied the influence of the double dipping process on the morphology of $MAPbI_3$, and longer dipping time caused more holes and defects on its surface. Finally, an optimized cyclic dipping process at 2×150 s leads to a flawless and high crystallinity $MAPbI_3$ layer, which can present an outstanding performance of the perovskite solar device of about 14%.

Data Availability

The data used to support the findings of this study are included within the article.

Conflicts of Interest

The authors declare that they have no conflicts of interest.

Authors' Contributions

Huy Anh Dinh and Thuy Thanh Thi Nguyen have the same contribution as the first authors.

Acknowledgments

This research is funded by the Vietnam National University HoChiMinh City (VNU-HCM) under grant number C2019-18-19. The authors are grateful to Prof. Tzu-Chien Wei for his instrument support and Dr. Bao-Long Hoang Nguyen for his discussion.

References

[1] T. K. Kojima, A. Y. Shirai, and T. Miyasaka, *Abstract#397, 210th ECS Meeting, Pennington, N.J*, Electrochemical Society, Cancun, Mexico, 2006.

[2] A. Kojima, K. Teshima, Y. Shirai, and T. Miyasaka, "Organometal halide perovskites as visible-light sensitizers for photovoltaic cells," *Journal of the American Chemical Society*, vol. 131, no. 17, pp. 6050-6051, 2009.

[3] J.-H. Im, C.-R. Lee, J.-W. Lee, S.-W. Park, and N.-G. Park, "6.5% efficient perovskite quantum-dot-sensitized solar cell," *Nanoscale*, vol. 3, no. 10, pp. 4088–4093, 2011.

[4] H. S. Kim, C. R. Lee, J. H. Im et al., "Lead Iodide Perovskite Sensitized All-Solid-State Submicron Thin Film Mesoscopic Solar Cell with Efficiency Exceeding 9%," *Scientific reports*, vol. 2, no. 1, p. 591, 2012.

[5] L. Etgar, P. Gao, Z. Xue et al., "Mesoscopic CH3NH3PbI3/-TiO2Heterojunction Solar Cells," *Journal of the American Chemical Society*, vol. 134, no. 42, pp. 17396–17399, 2012.

[6] M. M. Lee, J. Teuscher, T. Miyasaka, T. N. Murakami, and H. J. Snaith, "Efficient hybrid solar cells based on meso-superstructured organometal halide perovskites," *Science*, vol. 338, no. 6107, pp. 643–647, 2012.

[7] J.-Y. Jeng, Y.-F. Chiang, M.-H. Lee et al., "CH3NH3PbI3 perovskite/fullerene planar-heterojunction hybrid solar cells," *Advanced Materials*, vol. 25, no. 27, pp. 3727–3732, 2013.

[8] C. Mu, J. Pan, S. Feng, Q. Li, and D. Xu, "Quantitative Doping of Chlorine in Formamidinium Lead Trihalide (FAPbI 3– x Cl x) for Planar Heterojunction Perovskite Solar Cells," *Advanced Energy Materials*, vol. 7, p. 1601297, 2017.

[9] N.-G. Park, "Research direction toward scalable, stable, and high efficiency perovskite solar cells," *Advanced Energy Materials*, vol. 10, no. 13, p. 1903106, 2020.

[10] W. Zhang, M. Saliba, D. T. Moore et al., "Ultrasmooth organic–inorganic perovskite thin-film formation and crystallization for efficient planar heterojunction solar cells," *Nature communications*, vol. 6, no. 1, p. 6142, 2015.

[11] Q. Wei, W. Zi, Z. Yang, and D. Yang, "Photoelectric performance and stability comparison of MAPbI3 and FAPbI3 perovskite solar cells," *Solar Energy*, vol. 174, pp. 933–939, 2018.

[12] M. Wang, Y. Feng, J. Bian, H. Liu, and Y. Shi, "A comparative study of one-step and two-step approaches for MAPbI3 perovskite layer and its influence on the performance of mesoscopic perovskite solar cell," *Chemical Physics Letters*, vol. 692, pp. 44–49, 2018.

[13] B. A. Al-Asbahi, S. M. H. Qaid, M. Hezam, I. Bedja, H. M. Ghaithan, and A. S. Aldwayyan, "Effect of deposition method on the structural and optical properties of CH3NH3PbI3 perovskite thin films," *Optical Materials*, vol. 103, p. 109836, 2020.

[14] J.-H. Im, H.-S. Kim, and N.-G. Park, "Morphology-photovoltaic property correlation in perovskite solar cells: one-step versus two-step deposition of CH3NH3PbI3," *APL Materials*, vol. 2, no. 8, article 081510, 2014.

[15] Y. Fu, F. Meng, M. B. Rowley et al., "Solution growth of single crystal methylammonium lead halide perovskite nanostructures for optoelectronic and photovoltaic applications," *Journal of the American Chemical Society*, vol. 137, no. 17, pp. 5810–5818, 2015.

[16] Y. Luo, F. Meng, E. Zhao, Y.-Z. Zheng, Y. Zhou, and X. Tao, "Fine control of perovskite-layered morphology and composition via sequential deposition crystallization process towards improved perovskite solar cells," *Journal of Power Sources*, vol. 311, pp. 130–136, 2016.

[17] T.-Y. Hsieh, C.-K. Huang, T.-S. Su, C.-Y. Hong, and T.-C. Wei, "Crystal growth and dissolution of methylammonium lead iodide perovskite in sequential deposition: correlation between morphology evolution and photovoltaic performance," *ACS Applied Materials & Interfaces*, vol. 9, no. 10, pp. 8623–8633, 2017.

[18] H. Gao, X. Meng, Y. Du, and X. Gao, "Fabrication and characterization of perovskite CH3NH3PbI3 films via two-step sol-gel process: impact of soaking time of PbI2," *Thin Solid Films*, vol. 682, pp. 37–43, 2019.

[19] T. Baikie, Y. Fang, J. M. Kadro et al., "Synthesis and crystal chemistry of the hybrid perovskite (CH3NH3)PbI3 for solid-state sensitised solar cell applications," *Journal of Materials Chemistry A*, vol. 1, no. 18, pp. 5628–5641, 2013.

[20] Y. Ando, Y. Ohishi, K. Suzuki, A. Suzuki, and T. Oku, "Rietveld refinement of the crystal structure of perovskite solar cells using CH3NH3PbI3 and other compounds," in , Article ID 020003*AIP Conference Proceedings*, vol. 1929, Tokyo, Japan, 2018.